Power-Electronics-Based Energy Management System with Storage

Giovanna Oriti , Alexander L. Julian, Nathan J. Peck

K.Srinivas Head assistant professor ,WITS Warangal, M.Venkatesh M.Tech (PE) ,WITS Warangal.

Abstract—This paper demonstrates the functionality of a power-electronics-based energy management system (EMS). The EMS includes batteries and a digitally controlled single-phase voltage source inverter (VSI), which can be controlled as a current source or a voltage source depending on the status of the ac grid and the user's preference. The EMS guarantees that the critical loads are powered when the ac grid fails; in which case, the VSI is controlled as a voltage source. It also accomplishes peak power control by sup-plying battery power to the local loads while they are powered by the ac grid if the loads get large. The electricity cost savings accom-plished by peak shaving are estimated. The EMS functionality is demonstrated by experimental measurements on a laboratory pro-totype. The control architecture and logic embedded in the EMS are discussed in detail.

*Index Terms—***Energy management systems (EMS), energy stor-age, peak power control, voltage source inverters (VSI).**

I. Introduction

ENERGY savings and energy efficiency have become top priorities all around the world, stimulated by the Kyoto protocol and other pressing needs to reduce fossil fuel consump-tion. Additionally, energy security is a necessity for many in-stallations such as military bases and health care facilities where reducing energy consumption must be accomplished while keeping critical electrical loads serviced at all times.

In this paper, a power-electronics-based energy management system (EMS) is presented to accomplish peak power control in a single-phase power system while guaranteeing continuous service to critical loads at the same time. Peak power control, also known as peak shaving, is a method used to reduce the electricity charges for users with time of use (TOU) contracts and those who pay for the demand charges [1]. The power system does not need to be a microgrid, meaning that distributed generation (DG) does not need to be part of the power system. However, if DG units, such as photovoltaic panels or diesel generators, are part of the installation the EMS can manage these resources. The EMS proposed in this paper includes energy storage in the form of batteries in order to accomplish three main goals: 1) make electric power available to critical loads at all times with or without main grid service available, 2) reduce peak power consumption to lower electricity costs, and 3) store energy produced by DG units or during the time in which electricity from the grid is least expensive.

Recently researchers have used power converters to imple-ment power management or EMS for ac and dc microgrids. Results in the literature include power quality solutions [5], stabil-ity issues [6], high frequency microgrids [7], dc microgrids [8], [9], renewable generation interface [10]–[12], optimized third-level microgrid control (as described in [3]) with load and gener-ation forecast [13], [14]. Most publications have focused on the energy management of microgrids including several distributed resources (DR) [2], [15]–[18], while in this paper, we focus on managing a power system that includes battery storage. Fur-thermore, many referenced publications deal with three-phase systems, while this paper focuses on a single-phase-inverter-based EMS. Carnieletto *et al.* in 2011 [19], and more recently, Wai *et al.* [20] and de la Fuente *et al.* [21] have presented single-phase inverters for grid interface in both grid connected and stand-alone mode of operation. This paper, while following along the same line of research, introduces the prospective of continuous service to critical loads with peak power shaving. It also includes a simple economic analysis to demonstrate the ad-vantages of the peak power shaving method. While applications that emphasize energy security have been considered by Arnedo *et al.* in [22] and [23], the combination of energy security and energy cost reduction combined is new to these authors' knowl-edge. Furthermore, this paper presents simpler control systems and different topologies than those reported in [19] through [24]. Another innovative feature of the EMS presented in this paper is the use of a single off-the-shelf three-leg integrated power module to accomplish all the required tasks including battery charging, peak shaving, and fault tolerance.

II. EMS Architecture and Functionality

The EMS presented in this paper includes batteries and a three-leg power module controlled by a field programmable gate array (FPGA). The schematic in Fig. 1 depicts the EMS architecture. A three-phase IGBT power module is controlled to achieve buck and boost power flow from one leg of the module and single-phase voltage source operation (H-bridge inverter) from the other two legs of the module. The H-bridge inverter, thus, formed is connected to an output LC filter to produce the sinusoidal voltage for the ac loads. There are two voltage sensors to monitor the voltages v_{dc} and v_{ac}. There are two current sensors to monitor i_{ems} and i_{load}.

A battery pack is connected to the buck–boost leg to accom-plish bidirectional power flow to/from the battery. The battery consists of six, 12-V battery cells in series, forming a 72-V
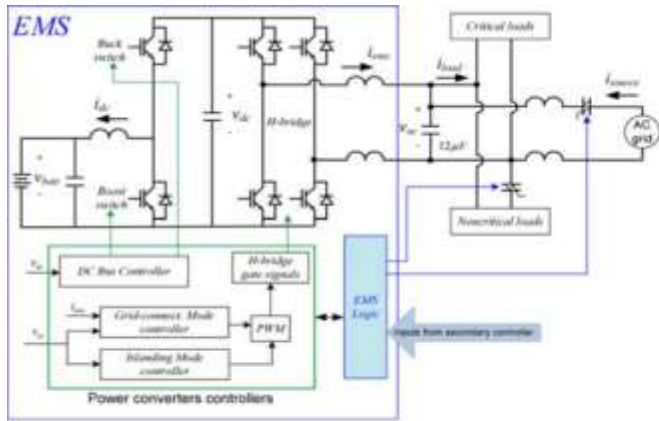
International Journal of Research

Available at https://edupediapublications.org/journals

e-ISSN: 2348-6848
p-ISSN: 2348-795X
Volume 05 Issue 15
May 2018

Fig. 1.   EMS architecture.

Fig. 2. EMS logic flowchart. Run, Charge, SC and CT are inputs from the operator or secondary controller.

battery pack. Note that a 300-V battery pack would eliminate the need for the buck/boost stage of the EMS, thus forming the dc bus for the H-bridge inverter. Critical loads are connected directly to the ac voltage created by the EMS, which is labeled $v_{a\,c}$ in Fig. 1. Critical loads are those loads that must be powered at all times because they are critical to the mission. Noncriti-cal loads are connected in parallel to $v_{a\,c}$, however, they can be shed when necessary using a thyristor switch. This increases the control of the power that can be directed to the critical loads when necessary. The ac grid can also be disconnected from $v_{a\,c}$ if needed to island the operation of the EMS. Typically islanding mode occurs when the ac grid fails. In this mode of operation, power to critical loads is guaranteed by drawing energy from the battery pack.

The EMS functionality is demonstrated in this paper by exper-imental validation with a laboratory prototype. The following scenarios are discussed:

1) peak shaving by tapping the energy storage system during high power demand;
2) islanding or stand alone mode of operation when the main ac grid is no longer available;
3) battery charging mode.

By accomplishing these goals, the EMS can be very useful in grid-connected systems, where there is a limit on the user's power consumption. This limit maybe enforced by circuit break-ers controlled by a power meter. If the EMS keeps the source current below a set threshold at all times by load management and shedding, then the user can operate loads beyond the steady-state power limits of the ac grid for short times without worrying about the circuit breaker interrupting service. The EMS can also be useful when the user has a TOU electricity contract with the power company and pays different rates for power delivered at different times of the day. In this case, the EMS can manage the energy stored and energy drawn from the grid to reduce consumption when the power rates are higher. This technique is known as load leveling [4] or retail energy time shift [25] and it achieves electricity cost reduction for the user. On an au-tonomous microgrid, where one or more generators are used to power different loads, the EMS allows derating of the generator
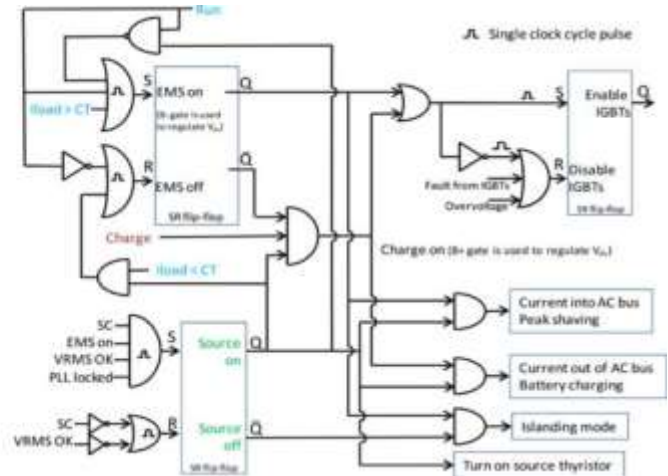
by controlling the peak root-mean-square (RMS) current drawn from the generator. It can also ensure power to critical loads is maintained during a fault by managing energy storage [26].

Unintentional islanding is undesirable and can be a safety problem during maintenance events. Future work will include testing the EMS as detailed in IEEE Std. 1547.1, paragraph 5.7.1 [27]. The prototype EMS developed so far is a small scale version of the target design. The next EMS will be designed to service a 20-A circuit, and for that hardware, we will accomplish the unintentional islanding testing.

The EMS control algorithm was developed with the following goals, listed here in order of priority:

1) power must be available to the critical loads at all times;
2) reduce the peak power absorbed by the microgrid by using battery power and by noncritical load shedding;
3) maximize the state of charge of the battery;
4) make power available to noncritical loads.

III. EMS CONTROL SYSTEMS

It is important to distinguish the different levels of control for the EMS. The primary control system includes the power con-verter module controllers, which generate the gate drive signals given reference voltages and currents. The secondary control system is a higher level controller, which can include the user input and makes decisions based on factors such as battery state of charge and lifetime, cost of electricity, time of day, load pri-ority, etc. This paper focuses on the primary control system. The basic functions of the primary controller are included in Fig. 1 and will be examined in details in this section.

Fig. 2 shows the EMS primary controller logic flowchart, which is a detailed visualization of the "EMS Logic" block in Fig. 1. The operator or the secondary controller inputs four dis-tinct logical commands; Run, Charge, Source Connect (SC), and Current Threshold (CT). CT is the load current level when the EMS will begin peak shaving. If Run is low, then the EMS does nothing. When Run is high, the EMS will operate in islanding
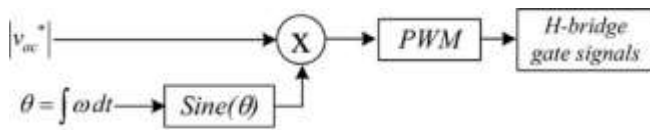
International Journal of Research

Available at https://edupediapublications.org/journals

e-ISSN: 2348-6848
p-ISSN: 2348-795X
Volume 05 Issue 15
May 2018

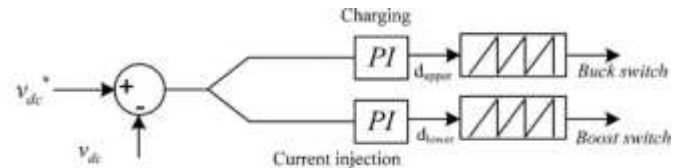Fig. 3.   Control algorithm for islanding mode.

Fig. 5.   DC-bus control algorithm.

B. EMS Control in Current Injection Mode

The EMS can provide several valuable grid support functions when the EMS is connected to an active ac grid. These modes of operation operate the EMS as a current source. Two current injection modes of operation are shown in Fig. 4.
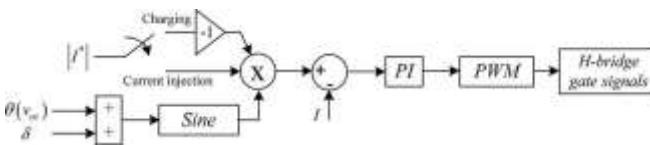
If the desired action is charging the batteries, then a reference current, I^*, defines the amplitude of the current to be drawn from the grid to charge the batteries. The electrical angle, θ ($v_{a\,c}$), is derived from the grid voltage using zero crossing detection of the EMS voltage, $v_{a\,c}$. The current drawn from the grid will typically be at unity power factor, which means that $\delta = 0$ in this mode of operation.

When the desired action is real or reactive power flow into the EMS ac bus, then the controller switches to current injection mode. The electrical angle chosen will dictate the amount of real or reactive power that will flow, as scheduled. When $\delta = 0$, the power factor is unity because θ ($v_{a\,c}$) is synchronized to the electrical angle of $v_{a\,c}$.

Fig. 4.   Control algorithm for current injection.

mode. If SC is also high, then the EMS will connect $v_{a\,c}$ to the ac source if the ac source RMS voltage is above 100 Vrms (voltage root mean square (VRMS) OK is high). If the load current exceeds the peak shaving limit (CT), then the EMS will continue to inject current, otherwise the EMS will turn OFF after connecting to the ac source. If charge is set high, then the EMS will charge the batteries when the ac source is present and peak shaving is not demanded.

There are two other internal variables: phase-locked loop (PLL) locked and VRMS OK. When the signal VRMS OK is high, the ac grid RMS voltage is above a set threshold. When this signal is low, the EMS switches from grid connect to islanding mode of operation.

These four commands coming from the secondary controller can be set based on several factors. The secondary control system will set the charging command and the peak shaving thresholds in order to achieve the best performance. The information that will be used by the higher level controller will include state-of-charge, time of day, cost of electricity, and other factors.

The different components of the EMS primary control system for the different modes of operation are presented in the following sections.

A. EMS Control in Islanding Mode

Islanding or stand-alone mode occurs when the ac grid is deenergized or the EMS is disconnected from the ac grid. The control algorithm for this mode of operation is shown in Fig. 3. The amplitude of the ac voltage, $v_{a\,c}*$, is set to 110 Vrms. The electrical angle, θ, is defined by integrating the angular fre-quency, which is set to 60 Hz. Unipolar pulse width modulation (PWM) is used to drive the H-bridge IGBTs. This open-loop control algorithm does not compensate for RMS output voltage deviations or provide any active damping but these capabilities are easily implemented as required.

C. DC-Bus Control Algorithm

The dc bus that powers the H-bridge and the buck–boost switches is controlled as shown in Fig. 5. Only one IGBT is modulated at any given time so that when the buck or boost converter is in discontinuous conduction mode, the current does not cross zero. This improves the efficiency compared to driving both switches all the time. Whenever battery charging mode is chosen, current is injected into the dc bus by the H-bridge and the dc-bus controller operates in buck mode to deliver the energy to the battery pack. When the EMS is in current injection mode, the power delivered to the ac bus is drawn from the dc bus and the dc-bus controller operates in boost mode to hold the dc bus up using battery power.

The IGBT module that is being used has charge pumps to provide energy to the IGBT gate drives. This is a significant simplification and cost saving feature of the power module. In order to energize the buck switch for battery charging, the boost switch must first be exercised to pump charge into the upper IGBT gate drive circuit. This is accomplished in about 500 μs just prior to charging mode.

IV. EMS HARDWARE IMPLEMENTATION

The EMS hardware is shown in Figs. 6 and 7. It includes a field programmable gate array FPGA development board [28] with input/output (I/O) ports, a three-phase insulated gate bipolar transistor (IGBT) power module, power supply, voltage/current sensors, analog/digital (A/D) converters, transistor–transistor logic (TTL) interface and an USB interface to communicate with a personal computer (PC). A Joint Test Action Group (JTAG or IEEE Standard 1149.1) programming cable interfaces the FPGA development board to a PC and is used to program the FPGA. The software development tool used for the FPGA is Simulink [29] with the addition of Xilinx System Generator software [30], which compiles the Simulink model to create VHDL code.

International Journal of Research

Available at https://edupediapublications.org/journals

e-ISSN: 2348-6848
p-ISSN: 2348-795X
Volume 05 Issue 15
May 2018

Fig. 8.   AC loads set up for laboratory experiments.
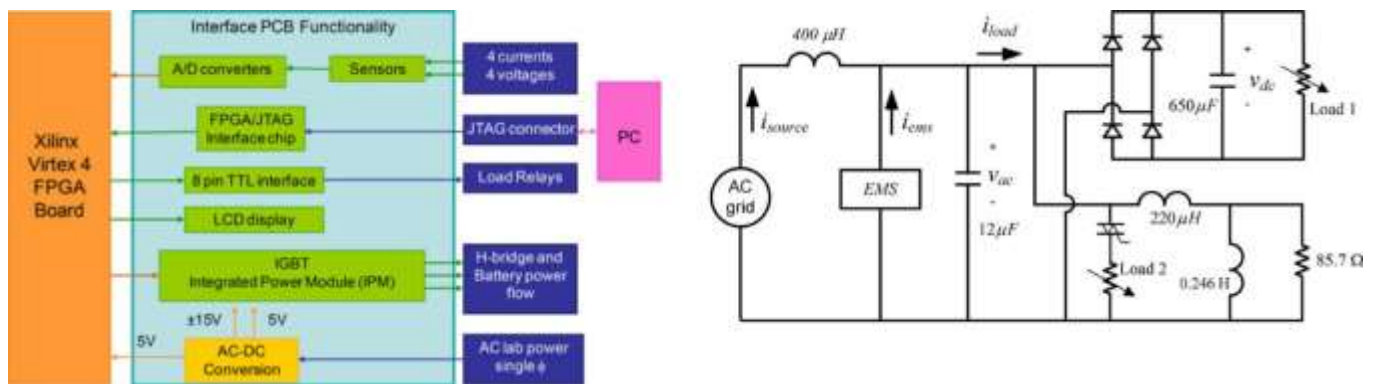
Fig. 6.   EMS hardware block diagram.

Fig. 7.   Photograph of EMS electronics as implemented in the laboratory.

The interface functionality of Fig. 6 is realized by two printed circuit boards (PCBs) mounted above and below the FPGA development board as shown in Fig. 7. The bottom PCB in-cludes the power components such as the IGBT integrated power module (IPM), current and voltage sensors, passive components, and dc power supply. The IGBT IPM includes six diodes, six IGBTs, and the gate drive circuits in the standard three-phase three-leg configuration. The PCB mounted on top of the FPGA development board includes an USB interface chip, USB con-nector to interface with the PC, A/D converters, voltage level shifters, and several other connectors to interface with the other boards.

V. Experimental Measurements

The circuit shown in Fig. 1 was built in the laboratory to demonstrate the EMS functionality. The ac voltage is $v_{ac} = 120$ Vrms, the battery pack voltage is $v_{batt} = 72$ Vdc and it is boosted to create the dc-bus voltage $v_{dc} = 200$ V for the H-bridge inverter. The EMS output filter shown in Fig. 1 includes a 12-μF capacitor and 1.16-mH inductance distributed on both sides of the capacitor. The loads include a diode rectifier and *RL* loads as shown in Fig. 8. The passive components can be
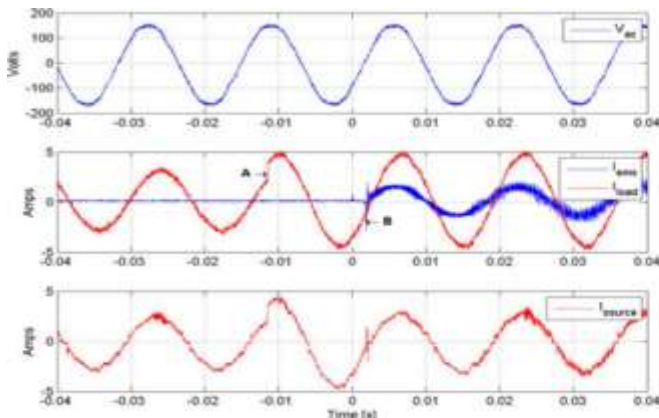
adjusted to create different load conditions. The objective of this section is to demonstrate the modes of operation of the EMS with load step changes.

A. Peak Shaving and Battery Charging With the AC Grid Connected

Residential and commercial TOU electricity rates include different rates at different time of the day (such as on-peak and off-peak) and also demand charges. Demand charges are based on the customer's peak demand on a given month, usu-ally averaged over a 15-min period [1]. TOU rates are devised by the power companies to encourage customer to shift their loads away from the peak demand times and in general reduce their peak power consumption. The ideal customer would draw constant power at all hours of the day. Reducing the peak power consumption results in significant cost savings. Peak shaving is a known technique [25], [31] used to achieve this objective by use of stored energy. Electrical energy is stored during the times when electricity cost is lowest (typically at night) and used dur-ing the times when electricity cost is highest, in order to reduce the overall electricity charges. While it may not be cost effective to acquire a battery pack with the sole purpose of peak shaving, if storage is part of an existing EMS installed to improve the reliability of the local power system, then using it to accomplish peak shaving is very cost effective as will be demonstrated in Section VI.

Peak shaving is achieved by controlling the RMS current in the load, which is related to the source current. A threshold is set for the load current, such that when the load RMS current exceeds this threshold, the EMS supplies some of the load cur-rent. This keeps the peak current drawn from the ac grid below a set limit. In the laboratory experiments presented here, the threshold for the load current is such that the peak shaving fea-ture turns ON when the load current is greater than 2.2 Arms and turns OFF when the load current is below 2.1 Arms. When peak shaving turns ON, the EMS behaves as a current source supplying to the load a sinusoidal current with unity power fac-tor. The threshold value can be changed by modifying the EMS reference current by the secondary controller. The EMS can be programmed to provide reactive power as well as current har-monics as needed by the user or the secondary controller. In this paper, however, only active power control is demonstrated.
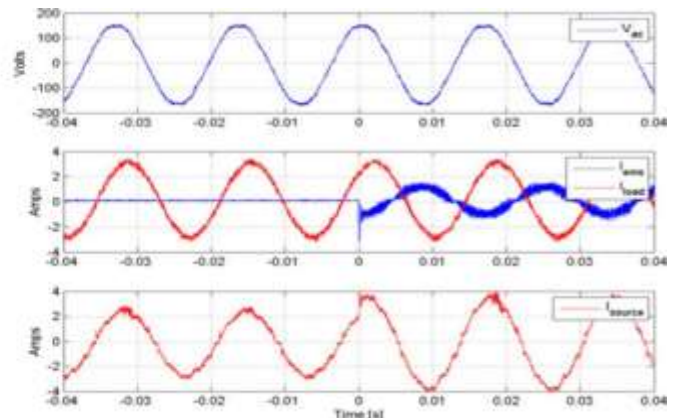
Fig. 9. Peak shaving with the EMS providing some of the load current from Fig. 11. EMS turning ON at $t = 0$ to charge the battery pack. the battery pack when the load increases. Load 2 steps from 600 to 80 Ω (A), and then, the EMS turns ON (B). All the loads are linear.

TABLE I
LOAD CONDITIONS FOR THE EXPERIMENTAL MEASUREMENTS IN
GRID-CONNECTED MODE

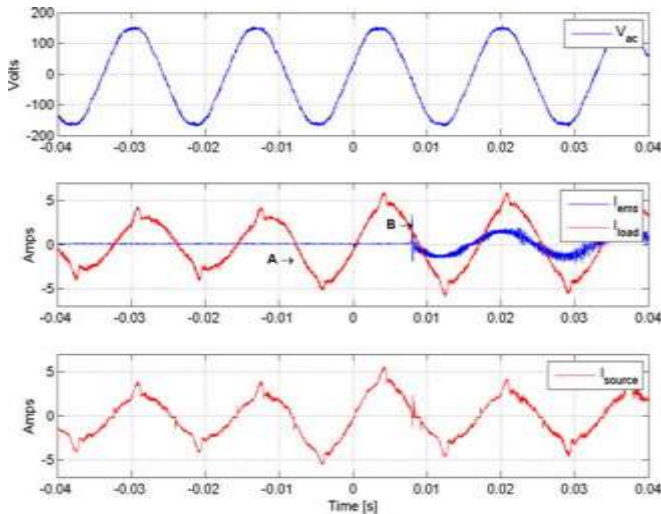|	Load 1	Load 2	AC grid
Fig. 9		Step from 600 to 80 Ω	ON
Fig. 10	1200 Ω	Step from 1200 to 85.7Ω	ON
Fig. 11		600 Ω	ON

Fig. 10. Peak shaving with the EMS providing some of the load current from the battery pack when the load increases. Load 2 steps from 1200 to 85.7 Ω (A), and then, the EMS turns ON (B). The load includes a diode rectifier.

Figs. 9 through 11 include the experimental waveforms obtained in ac grid-connected mode. Table I displays the values of the different loads used to create the waveforms in these figures. In Figs. 9 and 10, the turn ON of the EMS is demonstrated. The load current increases, and the EMS current supplies some of the current to reduce the peak power consumption from the grid. A step change in the load is implemented by changing "Load 2" in Figs. 9 and 10 as recorded in Table I. The only difference between the two sets of waveforms is that the diode rectifier is included in the load in Fig. 10, while it is not part of the load in Fig. 9. The diode rectifier is excluded from the circuit by making the variable resistor labeled as "Load 1" very large, indicated as Table I. It can be noted that the nonlinear load has a significant effect on the quality of the current waveforms but it does not change the dynamic of the EMS turn ON event. At this time, the EMS cannot compensate for the load current harmonics; future work will add this capability so that the source current can be made sinusoidal with non linear loads.

The EMS turns ON to charge the battery at $t = 0$ s in Fig. 11 as demonstrated by the EMS current $I_{em\ s}$ being 180° out of phase with respect to the ac voltage. As can be noted from Table I, only linear loads are used for this experiment, because the diode rectifier load is disabled. The battery charging mode of operation is allowed because the load is light, so the EMS does not need to provide an additional current for peak shaving. A secondary controller typically turns ON the battery charger when the cost of electricity is lowest and the loads are light, which happens a night in most cases.

There is a delay between the load increase and the EMS turning ON due to the RMS current computation algorithm, which is described in the next section.

B. EMS Powering Critical Loads When the AC Grid Fails—Islanding Mode of Operation

In order to provide power to critical loads when the ac grid fails, the EMS detects grid failure and acts as a voltage source for the critical loads. In this mode of operation, noncritical loads can be shed depending on the state of charge of the batteries and other factors determined by the user or by the secondary control system. Noncritical load shedding is easily accomplished by the EMS by opening the thyristor switch connected to the noncritical
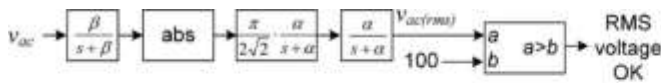
Fig. 12.   RMS voltage monitoring system block diagram.

loads (shown in Fig. 1). When the ac grid is available again, then the EMS restores the loads to the ac grid, therefore, terminating the islanding mode of operation. At this point, if noncritical loads had been previously disconnected they can be restored as determined by the secondary control system. The secondary control system determines if the EMS should try to reconnect to the ac grid or not.

The RMS voltage of the ac bus is monitored to detect when islanding mode is needed. If the RMS voltage drops below 100 Vrms, then the EMS opens the thyristor connecting the grid to the ac bus (shown in Fig. 1) and the EMS switches to islanding mode. This is another programmable feature that can be managed by a higher level controller. There is a delay in the detection of the loss of the source due to a low-pass filter used in the detection algorithm. The detection algorithm is shown in Fig. 12. First v_{ac} is filtered at a corner frequency of $\beta = 700\pi$ radians per second. Next, the absolute value of the ac voltage is put through α low-pass filter with a corner frequency a that can be adjusted in order to change the speed of transition from grid connect to islanding mode. In the experimental measurements presented below, $\alpha = 20\pi$ and $\alpha = 60\pi$ radians per second are

used with different results. The gain factor of $\pi/2\sqrt{2}$ yields the exact value for the RMS voltage when v_{ac} is a sine wave and α is small because

$$\frac{\pi}{2\sqrt{2}}avg(/V/) = \frac{\pi}{2\sqrt{2}}\frac{1}{\pi}\int_0^\pi V\sin(\theta)\,d\theta = \frac{\pi}{2\sqrt{2}}\frac{2V}{\pi} = V_{rms}. \quad (1)$$

The estimated RMS voltage is compared to 100 V and sets the logical decision for the RMS voltage level. This decision is used by the logic shown in Fig. 2 to determine the operating mode of the EMS. This algorithm requires less computation than the RMS algorithm yet introduces only a small error. There is a delay in the detection of the loss of the ac source; however, false alarms due to momentary notching of the ac bus do not cause the EMS to disconnect from the source.

The experimental waveforms in Figs. 13 through 15 show how the EMS enters and exits the islanding mode of operation. In grid-connected mode, the EMS is always monitoring the phase angle of the ac source. When the RMS voltage falls below a set threshold (100 V), the EMS interprets the event as a grid failure and switches to islanding mode of operation. Table II displays the load conditions for the experimental set up used to obtain the waveforms in the three figures. Grid failure with EMS turning ON is demonstrated in Figs. 13 and 15 with two different corner frequencies for the low-pass filter of the RMS voltage monitoring system shown in Fig. 12. Increased frequency results in faster

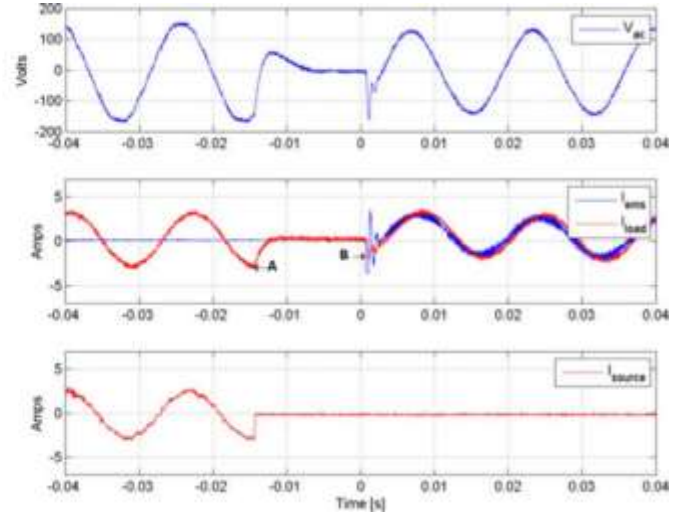transient response. The return to ac grid-connected mode is demonstrated in Fig. 14.

Fig. 13. Experimental waveforms showing ac grid failure (A) and the EMS taking the loads into islanding mode (B). $\alpha = 20\pi$.

TABLE II
LOAD CONDITIONS FOR TRANSITIONS IN AND OUT OF ISLANDING MODE OF OPERATION

	Load 1	Load 2	α (rad/s)	AC grid
Fig. 13		600 Ω	20 π	ON to OFF
Fig. 14		600 Ω	20 π	OFF to ON
Fig. 15		600 Ω	60 π	ON to OFF

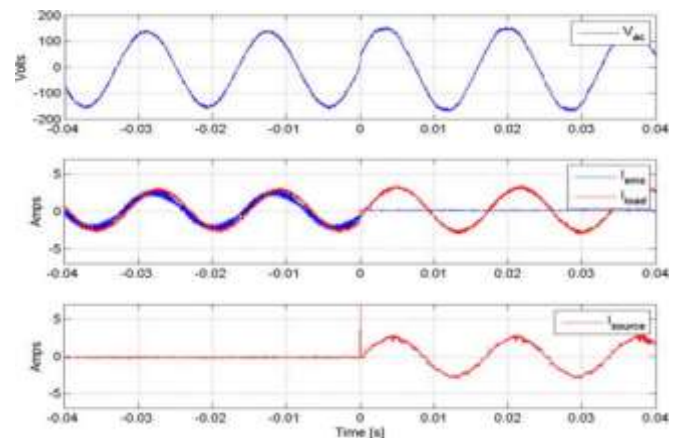The corner frequency α of the filter in the RMS voltage monitor-ing system is also changed.

Fig. 14.   Experimental waveforms showing the ac grid being restored at $t = 0$.

The difference between the marked points "α" and "B" in Figs. 13 and 15 shows the impact that the low-pass filter corner frequency a has on the dynamic response of the EMS to grid failure. The loss of source delay (B-A) is 15.1 ms in Figs. 13 and 5.7 ms in 15. Clearly the fast response is preferred for a smoother transition from grid-connect to islanding mode of
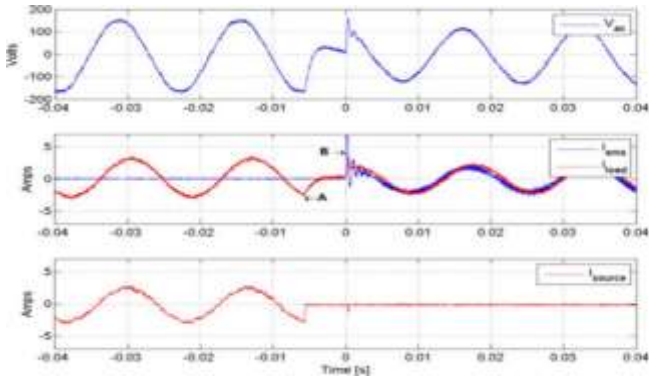
International Journal of Research

Available at https://edupediapublications.org/journals

e-ISSN: 2348-6848
p-ISSN: 2348-795X
Volume 05 Issue 15
May 2018

Fig. 15. Experimental waveforms showing ac grid failure (A) and the EMS taking the loads into islanding mode (B). $\alpha = 60\pi$.

Fig. 16. Power flow diagram with an EMS implementing peak shaving.

TABLE III
LIST OF TERMS USED IN THE POWER BALANCE ANALYSIS

P_{ems}	Power from the AC grid Charging power into
P_{ch}	EMS Discharging power out of EMS
P_{dis}	Charging power into battery after losses
P_{bin}	Discharging power out of battery before
P_{bout}	losses Efficiency of the EMS and the batteries
η	

operation. However, the drawback of a fast response time is that islanding mode could occur even if there is no loss of power, but simply a voltage notch. Of course, this could be desirable depending on the sensitivity of the loads being serviced.

The disturbance in the voltage waveform is noticeable when the EMS reconnects the ac grid to the loads as shown in Fig. 14. There is also an inrush current into the diode rectifier because the dc voltage of the rectifier had sagged some during islanding mode. Note that the ac voltage produced by the EMS during the islanding mode is slightly smaller (about 7%) than the ac grid voltage. This was intentionally done in order to distinguish the EMS-produced voltage from the ac grid voltage during the ex-perimental measurements. When the EMS reconnects the loads to the ac grid, it is already phase locked to the grid voltage as shown in Fig. 14.

VI. APPLICATION AND ECONOMIC CONSIDERATIONS

An EMS can be embedded in a building's power system to guarantee continuous service to critical loads when the ac grid is down. In addition, the EMS can reduce the cost of electricity by implementing peak shaving as described in this paper. The concept is simple and well known [25], [31]. It involves storing electrical energy when the cost of energy is low and utilizing the stored energy when the cost of energy is high. An additional benefit is that demand charges, which are based on maximum load during the peak demand period, can be reduced as well. The energy stored can come from the ac grid during off peak hours or from DG such as photovoltaic arrays, fuel cells, gas generators, or wind turbines, as examples. In this paper, the former scenario is studied.

This section presents an estimate of the electricity cost savings obtained with peak shaving. The facility's electricity contract is assumed to be of the TOU type, which is typical for commercial and industrial customers, where the cost of electricity is higher during the central hours of the day (i.e., 12:00 noon to 6:00 PM) and lower during the remaining hours. As the electricity rates
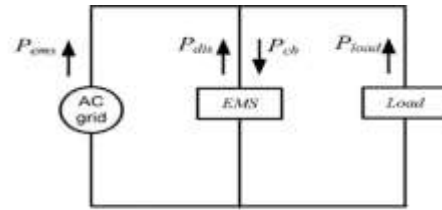
vary depending on location and different seasons, the per unit (pu) metrics will be used here. The size of the battery pack de-pends on the discharge duration range (how long the batteries are required to supply power to the loads continuously) and on the targeted lifetime of the system. For this analysis, we are using the assumption that there are two TOU rates: peak and off peak, neglecting the "partial peak" rates in order to simplify the analysis. The goal is to show the advantage of using an EMS to reduce electricity expenses in facilities where typical buildings have medium to large commercial TOU electricity contracts. It must be pointed out that the EMS system cost is not estimated in this paper, therefore, the return on investment is not com-puted. The reason for neglecting the cost of the EMS system is due to the assumption that the system is embedded in the fa-cility's power system for reliability purposes, specifically to guarantee continuous service to critical loads, so it is presumed to be there for reasons other than reducing the cost of electric-ity. Therefore, reducing the electricity bill is viewed here as an additional benefit, not the primary reason for installing an EMS.

Power balance, conservation of energy, and the EMS effici-ency are used to demonstrate how charging and later discharging the batteries can save money when the electricity rates change based on a TOU profile. The power relationships for the diagram in Fig. 16 are described in (2) and in Table III.

The battery pack is included in the EMS block; the battery power stored and later used is included in this analysis and the EMS/battery efficiency is considered in the performance

$$P_{ems} = P_{ch} - P_{dis} + P_{load} \qquad (2)$$

Fig. 17 shows an example of how the EMS $\frac{P_{bin}}{\eta}$ can be used to reduce the power drawn from the ac grid during peak hours, when the rates are higher. The TOU rates, in pu, are represented by the continuous line. The dashed line is the power consumed by the loads without the EMS, while the dashed-dotted line

International Journal of Research

Available at https://edupediapublications.org/journals

e-ISSN: 2348-6848
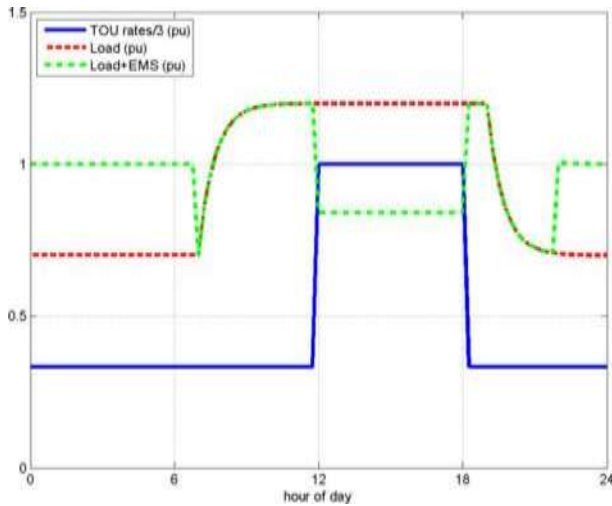p-ISSN: 2348-795X
Volume 05 Issue 15
May 2018

Fig. 17. TOU rates and power consumption with and without EMS.

represents the power drawn from the ac grid when the EMS is functioning. Power is drawn during off peak hours to charge the batteries and it is then released during peak hours to reduce the peak power consumption from the ac grid. Energy balance is included when plotting the load+EMS curve, including losses due to the power conversion in the EMS. Thus, the sum of the areas below the charging curves (off peak hours) plus the losses is equal to the area above the discharging curve (peak hours).

The daily cost of electricity can be quantified as a func-tion of the cost for electricity and the instantaneous power consumption

$$\$/\text{day} = \int_0^{24\,hours} \$/\text{kWh}(t) \cdot p(t)dt \tag{3}$$

where \$/day is the cost of electricity per day, \$/kWh(t) is the cost per kWh as a function of time and $p(t)$ is the power consumed by the load and EMS. Equation (3) shows that the daily cost of electricity can be minimized by minimizing the amplitude of the integrand, which is the product of the electricity cost and the power being consumed. Energy conservation is the first step to reduce cost. Energy conservation will make $p(t)$ as small as possible. Next, if the power can be consumed when the energy cost is lower, this will reduce the electricity bill. As a third step, energy can be stored when it is cheaper and used when it is more expensive if the consumption cannot be moved to a different time. This is the function that the EMS accomplishes.

The load curves plotted in Fig. 17 can be used to compute daily cost savings given electricity rates and load power consumption. Specifically, given the daily cost of electricity from (3), the actual cost per day can be obtained

$$\$/\text{day} \cdot \$_{actual}/\text{kWh} \cdot P_{rated\_load} = \$_{actual}/\text{day} \tag{4}$$

where $\$_{actual}/\text{kWh}$ is the actual cost of electricity per kWh and $P_{rated\ load}$ is the rated power of the load.

For example, using 0.17\$/kWh, 500 kW = 1 pu rated power and an EMS efficiency of 90%, a daily cost saving of 10% is accomplished using the EMS. This savings is realized with an EMS that is only delivering 0.3 pu power as shown in Fig. 17.

Further economic analysis can yield more details and can show how the cost savings change as a function of the electricity rates, seasons, power rating, and efficiency. The addition of demand charges into the analysis would show that using an EMS yields even greater savings than demonstrated in this simple example. The solution shown in Fig. 17 reduces the demand during peak hours (1200–1800) but does not address the demand during off peak hours, which is planned for future analysis.

VII. CONCLUSION

In this paper, the functionality of a power-electronics-based EMS is demonstrated with a laboratory prototype. The control system designed to perform the experimental implementation of typical scenarios is presented in detail. Experimental data are shown to demonstrate how the EMS supports critical loads when the ac grid becomes unavailable and how the connection to the ac grid is restored by the EMS when the ac grid becomes available again. Additionally, the EMS can accomplish other advantageous tasks such as peak shaving. Experimental mea-surements with linear and nonlinear loads demonstrate how the EMS, controlled in current mode, provides some of the power to the loads to accomplish peak shaving, thus reducing the cost of electricity. A simple economic analysis is provided in support of this statement.

REFERENCES

[1] G. M. Masters, *Renewable and Efficient Electric Power Systems*. New York, NY, USA: Wiley 2004.

[2] *IEEE Standard for Interconnecting Distributed Resources With Electric Power Systems*, IEEE Std. 1547, 2003.

[3] J. Rocabert, A. Luna, F. Blaabjerg, and P. Rodriguez, "Control of power converters in AC microgrids," *IEEE Trans. Power Electron.*, vol. 27, no. 11, pp. 4734–4749, Nov. 2012.

[4] S. Vazquez, S. M. Lukic, E. Galvan, L. G. Franquelo, and J. M. Carrasco, "Energy storage systems for transport and grid applications," *IEEE Trans. Ind. Electron.*, vol. 57, no. 12, pp. 3881–3895, Dec. 2010.

[5] F. Wang, J. L. Duarte, and M. A. M. Hendrix, "Grid-Interfacing con-verter systems with enhanced voltage quality for microgrid application— Concept and implementation," *IEEE Trans. Power Electron.*, vol. 26, no. 12, pp. 3501–3513, Dec. 2011.

[6] E. Barklund, N. Pogaku, M. Prodanovic, C. Hernandez-Aramburo, and T. C. Green, "Energy management in autonomous microgrid using stability-constrained droop control of inverters," *IEEE Trans. Power Elec-tron.*, vol. 23, no. 5, pp. 2346–2352, Sep. 2008.

[7] S. Chakraborty, M. D. Weiss, and M. G. Simoes,˜ "Distributed intelli-gent energy management system for a single-phase high-frequency AC microgrid," *IEEE Trans. Ind. Electron.*, vol. 54, no. 1, pp. 97–109, Feb. 2007.

[8] Y. Chen, Y. Wu, C. Song, and Y. Chen, "Design and implementation of energy management system with fuzzy control for DC microgrid systems," *IEEE Trans. Power Electron.*, vol. 28, no. 4, pp. 1563–1570, Apr. 2013.

[9] B. I. Rani, G. S. Ilango, and C. Nagamani, "Control strategy for power flow management in a PV system supplying DC loads," *IEEE Trans. Ind. Electron.*, vol. 60, no. 8, pp. 3185–3194, Aug. 2013.

[10] J. M. Carrasco, L. G. Franquelo, J. T. Bialasiewicz, E. Galvan, R. C. P. Guisado, M. A. M. Prats, J. I. Leon, and N. Moreno-Alfonso, "Power-electronic systems for the grid integration of renewable en-ergy sources: A survey," *IEEE Trans. Ind. Electron.*, vol. 53, no. 4, pp. 1002–1016, Aug. 2006.

[11] P. Sun, C. Liu, J. Lai, and C. Chen, "Grid-tie control of cascade dual-buck inverter with wide-range power flow capability for renewable energy applications," *IEEE Trans. Power Electron.*, vol. 27, no. 4, pp. 1839–1849, Apr. 2012.

[12] C. Cecati, C. Citro, A. Piccolo, and P. Siano, "Smart operation of wind tur-bines and diesel generators according to economic criteria," *IEEE Trans. Ind. Electron.*, vol. 58, no. 10, pp. 4514–4525, Oct. 2011.

[13] H. Kanchev, D. Lu, F. Colas, V. Lazarov, and B. Francois, "Energy man-agement and operational planning of a microgrid with a PV-based active generator for smart grid applications," *IEEE Trans. Ind. Electron.*, vol. 58, no. 10, pp. 4583–4592, Oct. 2011.

[14] A. Chaouachi, R. M. Kamel, R. Andoulsi, and K. Nagasaka, "Multiob-jective intelligent energy management for a microgrid," *IEEE Trans. Ind. Electron.*, vol. 60, no. 4, pp 1688–1699, Apr. 2013.

[15] H. Zhou, T. Bhattacharya, D. Tran, T. S. T. Siew, and A. M. Khambadkone, "Composite energy storage system involving battery and ultracapacitor with dynamic energy management in microgrid applications," *IEEE Trans. Power Electron.*, vol. 26, no. 3, pp. 923–930, Mar. 2011.

[16] F. Z. Peng, Y. W. Li, and L. M. Tolbert, "Control and protection of power electronics interfaced distributed generation systems in a customer-driven microgrid," in *Proc. IEEE Power Energy Syst. Gen. Meet.*, 2009, pp. 1–8.

[17] F. Blaabjerg, Z. Chen, and S. B. Kjaer, "Power electronics as efficient interface in dispersed power generation systems," *IEEE Trans. Power Electron.*, vol. 19, no. 5, pp. 1184–1194, Sep. 2004.

[18] K. T. Tan, P. L. So, Y. C. Chu, and M. Z. Q. Chen, "Coordinated control and energy management of distributed generation inverters in a microgrid," *IEEE Trans. Power Del.*, vol. 28, no. 2, pp. 704–713, Apr. 2013.

[19] R. Carnieletto, D. I. Brandao,˜ S. Suryanarayanan, F. A. Farret, and M. G. Simoes,˜ "Smart grid initiative," *IEEE Ind. Appl. Mag.*, vol. 17, no. 5, pp. 27–35, Sep./Oct. 2011.

[20] R.-J. Wai, C.-Y. Lin, Y.-C. Huang, and Y.-R. Chang, "Design of high-performance stand-alone and grid-connected inverter for distributed generation applications," *IEEE Trans. Ind. Electron.*, vol. 60, no. 4, pp. 1542–1555, Apr. 2013.

[21] D. V. de la Fuente, C. L. T. Rodr´ıguez, G. Garcera,´ E. Figueres, and R. O. Gonzalez,´ "Photovoltaic power system with battery backup with grid-connection and islanded operation capabilities," *IEEE Trans. Ind. Electron.*, vol. 60, no. 4, pp. 1571–1581, Apr. 2013.

[22] L. Arnedo, S. Dwari, V. Blasko, and A. Kroeber, "Hybrid solar inverter based on a standard power electronic cell for microgrids applications," in *Proc. IEEE 2nd Energy Convers. Conf. Expo.*, Phoenix, AZ, USA, Sep. 2011, pp. 961–967.

[23] L. Arnedo, S. Dwari, V. Blasko, and A. Kroeber, "Hybrid solar inverter based on a standard power electronic cell for microgrids applications," in *Proc. IEEE Appl. Power Electron. Conf.*, Orlando, FL, USA, Feb. 2012, pp. 270–276.

[24] Z. Yao, L. Xiao, and Y. Yan, "Seamless transfer of single-phase grid in-teractive inverters between grid-connected and stand-alone modes," *IEEE Trans. Power Electron.*, vol. 25, no. 6, pp. 1597–1603, Jun. 2010.

[25] SANDIA Report SAND2013–5131. (2013, Oct.). *DOE/EPRI 2013 Electricity Storage Handbook in Collaboration with NECA.* [Online]. Avail-able: http://www.sandia.gov/ess/publications/SAND2013–5131.pdf

[26] R. L. Kelly, A. L. Julian, and G. Oriti, "Reducing fuel consumption at a remote military base—Introducing an energy management system," *IEEE Electrification Mag.*, vol. 1, no. 2, pp. 30–37, Dec. 2013.

[27] *IEEE Standard Conformance Test Procedures forEquipment Interconnect-ing Distributed Resources With Electric Power Systems*, IEEE Std. 1547.1, 2005.

[28] Xilinx. Avnet Virtex-4 LC Development Board. (2013, Feb.). [Online]. Available: http://www.xilinx.com/products/devkits/DS-KIT-4VLX25LC.htm

[29] Simulink by MathWorks. (2015, Mar.). [Online]. Available: http://www.mathworks.com/products/simulink/

[30] Xilinx. (2008, Mar.). System Generator for DSP—Getting Started Guide. [Online]. Available: http://www.xilinx.com/support/sw_manuals/sysgen_gs.pdf

[31] M. Bragard, N. Soltau, S. Thomas, and R. W. De Doncker, "The balance of renewable sources and user demands in grids: power electronics for modular battery energy storage systems," *IEEE Trans. Power Electron.*, vol. 25, no. 12, pp. 3049–3056, Dec. 2010.

Giovanna Oriti (S'94–M'97–SM'04) received the Laurea (Hons.) and Ph.D. degrees in electrical engi-neering from the University of Catania, Catania, Italy, in 1993 and 1997, respectively.

She was a Research Intern at the University of Wisconsin-Madison, Madison, WI, USA, for two years. After graduation, she joined United Technol-ogy Research Center, where she developed innova-tive power converter topologies and control. In 2000, she launched her own consulting business developing physics-based models of power converters and drives for electromagnetic interference analysis, stability analysis, and development of control algorithms. In April 2008, she joined the faculty of the Electrical and Computer Engineering Department, Naval Postgraduate School, Monterey, CA, USA, where she is currently an Associate Professor. She is involved in electric ship systems and energy management research activities. She holds one U.S. Patent and has coauthored more than 40 papers published in IEEE Transactions or IEEE conference proceedings.

In 2011–2012, she served as the Chair of the Industrial Power Conversion System Department, IEEE Industry Application Society. She received the 2002 IEEE IAS Outstanding Young Member Award. In 2012, she received the NPS ECE Service Award in recognition of her contribution to the development of the new NPS EE Energy curriculum.

Alexander L. Julian (S'91–M'98) received the B.S.E.E. and M.S.E.E. degrees from the University of Missouri, Columbia, MO, USA, in 1991 and 1992, respectively, and the Ph.D. degree in electrical engi-neering from the University of Wisconsin-Madison, Madison, WI, USA, in 1998.

In March 2004, he joined the Faculty of the Naval Postgraduate School (NPS), Monterey, CA, USA, as an Assistant Professor at the Electrical and Computer Engineering Department, Graduate School of Engi-neering and Applied Sciences. Before joining NPS, he contributed to shipboard electronic designs and research for many years as a consultant to Navy vendors by designing, modeling, and prototyping power electronics and motion control systems for many Navy applications. His research interests include solid-state power converter design and control, electromagnetic interference, reliability analysis, and stability analysis for distributed power sys-tems.

He holds four U.S. patents and has coauthored more than 40 papers in IEEE Transactions or IEEE conference proceedings.

Nathan J. Peck received the B.S. degree in electrical engineering from the United States Naval Academy, Annapolis, MD, USA, in 2005 and the M.S. degree in electrical engineering from the Naval Postgraduate School, Monterey, CA, USA, in 2013.

He has served aboard the submarine USS Jimmy Carter, and is currently the Engineer aboard the sub-marine USS Hampton, San Diego, CA, USA.